Joint Learning of Measurement Matrix and Signal Reconstruction via Deep Learning

Robiulhossain Mdrafi, *Student Member, IEEE*, and Ali Cafer Gurbuz, *Senior Member, IEEE*

***Abstract*—In this work, we propose an automatic sensing and reconstruction scheme based on deep learning within the compressive sensing (CS) framework. Classical CS utilizes pre-determined linear projections in the form of random measurements and convex optimization with a known sparsity basis to reconstruct signals. Here, we develop a data-driven approach to learn both the measurement matrix and the inverse reconstruction scheme for a given class of signals, such as images. The developed deep learning approach paves the way for end-to-end learning and reconstruction of signals with the aid of cascaded fully connected and multistage convolutional layers with a weighted loss function in an adversarial learning framework. Results obtained over the CIFAR-10 image database show that the proposed deep learning architectures provide higher peak signal-to-noise ratio (PSNR) levels, and, hence, learn better measurement matrices than that of randomly selected, specifically designed to reduce average coherence with a given basis, or state-of-the-art data driven approaches. The learned measurement matrices achieve higher PSNR compared to random or designed matrices not only when they are utilized in the proposed data-driven approach but also when used in ℓ_1 based recovery. The reconstruction performance on the test dataset improves as more training samples are utilized. Quantitative results for sparsity level analysis, incremental measurement design, and various training scenarios are provided.**

***Index Terms*—Measurement matrix design, deep learning, compressive sensing, learning sparse representation, convolutional neural networks, inverse problem.**

I. Introduction

THE generalized set of linear measurements defined by a measurement matrix (MM) plays a very crucial role in diverse areas of data science and sensing applications, such as imaging systems, radar and remote sensing, and wireless communications networks, where the compressed sensing (CS) [1]–[3] framework enables theoretical guarantees for sparse signal reconstruction. CS relies on two fundamental principles; namely, sparsity and incoherent sampling. The sparsity principle is built on the assumption that we can express a signal $\mathbf{x} \in R^{N\times 1}$ as a linear combination of K columns from an exactly known basis $\mathbf{\Psi} \in R^{N\times N}$ as $\mathbf{x} = \mathbf{\Psi s}$, where $\|\mathbf{s}\|_0 = K$ and $K \ll N$. Classical CS acquires random linear projections of the signal as $\mathbf{y} = \mathbf{\Phi x}$, with $\mathbf{y} \in R^{M\times 1}$ and $M \ll N$, while entries of the MM $\mathbf{\Phi}$ can be randomly selected from a given distribution, such as Gaussian or Bernoulli. In [4], a sufficient condition for the recovery of a K-sparse signal using orthogonal matching pursuit (OMP) [5] in terms of the mutual coherence of system $\mathbf{A} = \mathbf{\Phi\Psi}$ is provided as

$$\mu(\mathbf{A}) \leq \frac{1}{2K-1}, \tag{1}$$

where the mutual coherence $\mu(\mathbf{A})$ is defined as

$$\mu(\mathbf{A}) = \max_{k\neq l} \frac{|\mathbf{a}_k^T \mathbf{a}_l|}{\|\mathbf{a}_k\|_2 \|\mathbf{a}_l\|_2}, \tag{2}$$

representing the worst case coherence between any two columns of $\mathbf{A}$. Although fixed random linear MMs can be referred as universal in the sense that they can provide incoherence with many known basis, they are not specific and optimal to the underlying structure of the observed class of signals defined by the sparsity basis $\mathbf{\Psi}$.

The upper bound in (1) shows that for the same measurement number, we can obtain a better reconstruction of the observed signal, hence a larger K, by minimizing the mutual coherence $\mu(\mathbf{A})$. To achieve such a goal, there have been studies on the design of the MM, $\mathbf{\Phi}$. While some studies focus on constructing deterministic linear embedding using nuclear norm minimization with max-norm constraints [6], many studies have been focused on minimizing the averaged mutual coherence instead of the worst case coherence, defined in (2), under the assumption that the averaged metric will reflect an average signal recovery performance [7]–[9]. To this end, an iterative procedure was detailed in [7] to reduce the average mutual coherence of system $\mathbf{A}$ and results showed that the optimization of the projection matrix could provide improved recovery performance compared to a randomly generated MM. A similar goal is formulated to make the Gram matrix $\mathbf{G} = \mathbf{A}^T\mathbf{A}$ as close to the identity matrix as possible in terms of the Frobenius norm,

$$\min_{\mathbf{\Phi}} \ \|\mathbf{I} - \mathbf{\Psi}^T\mathbf{\Phi}^T\mathbf{\Phi\Psi}\|_F^2. \tag{3}$$

An iterative technique was proposed in [8] to solve (3), while a closed form solution to (3) was given in [9], which can be expressed as,

$$\mathbf{\Phi} = \mathbf{\Gamma\Lambda}^{-1/2}\mathbf{U}^T \tag{4}$$

with the assumption of $\mathbf{\Psi}$ being full rank. where $\mathbf{\Gamma}$ is any matrix with orthonormal rows such as $\mathbf{\Gamma} = [\mathbf{I_M}\ \mathbf{0}]$ and $\mathbf{U\Lambda U^T}$ is the eigenvalue decomposition of $\mathbf{AA}^T$. In [10], the result in

Manuscript received July 21, 2019; revised December 9, 2019 and February 28, 2020; accepted March 15, 2020. Date of publication March 30, 2020; date of current version April 27, 2020. This work was supported in part by National Science Foundation CPS program under Grant 1931861. The associate editor coordinating the review of this manuscript and approving it for publication was Dr. Singanallur Venkatakrishnan. *(Corresponding author: Ali Cafer Gurbuz.)*

The authors are with the Department of Electrical and Computer Engineering, Mississippi State University, Mississippi, MS 39762 USA (e-mail: rm2232@msstate.edu; gurbuz@ece.msstate.edu).

Digital Object Identifier 10.1109/TCI.2020.2983153

(4) is extended for a wider range of dictionaries. Mainly, we can obtain a specifically designed MM by utilizing one of the mentioned MM design techniques for an assumed sparsity basis $\mathbf{\Psi}$ to achieve a system with lower average mutual coherence as compared to that attainable with randomly selected MMs.

However, it might not always be possible to know the sparsity basis exactly since the inverse transform between the sensor data and the signal/image domain is not fully known due to sensor modelling errors and non-idealities, unknown propagation mediums, noise, and off-grid effects for different applications. In addition, generally, the signals are not exactly sparse in the assumed basis but only compressible. Moreover, MM design techniques try to minimize an average coherence metric, but this does not necessarily guarantee better signal reconstruction. Once the MMs and the sparsity dictionaries are chosen CS inherently defines a fixed assumed linear relation between the measurement and the signal domains. The main goal of an inversion technique is to use this assumed relation, which might come from prior domain knowledge, to reconstruct the signals.

Another possible approach to derive the actual unknown inverse relation from measurement to signal spaces is through exploiting the large, available, signal datasets. Recently, advances in data science, especially automatic feature learning with deep neural networks (DNNs) and its variants [11]–[14], have resulted in improved performance across many applications, including computer vision [15]–[17], and has prompted researchers to apply DNNs for a variety of inverse problems [18]. While analytical methods like CS require prior domain knowledge that can be incorporated into the solution, in contrast, DNNs exploit large datasets to derive the unknown solution to the inverse problem. In this work, we propose a data-driven approach inspired from sparse data acquisition and reconstruction techniques to learn both the MM and the DNN-based inverse reconstruction scheme for a given class of signals. The developed DNN features cascaded fully connected and multistage convolutional layers with a weighted loss function from each stage in an adversarial learning framework. Next, we briefly present the background on DNN-based reconstruction techniques and introduce the proposed ideas in learning of MM and signal reconstruction scheme with the novel main contributions of the work.

Studies into data driven learning of signal reconstruction has only recently been considered in the literature. One of the first studies in this area is presented in [19] implementing a stacked denoising autoencoder (SDA). However, the architecture of SDA involves cascaded sets of fully connected (FC) layers that make the training process computationally expensive with the increment of signal size. In addition, it also runs the risk of overfitting the testing set. To avoid the shortcomings of SDA, several improvements to the network structure are proposed in [20]–[24] mainly to reduce the high number of parameters of SDAs. In [20], a convolutional neural network (CNN) structure is learned between the image proxy obtained through the adjoint operator on the compressed measurements, i.e., $\mathbf{\Phi}^T\mathbf{y}$, and the actual image, where a fixed random MM is used to create the measurements. In [21], a FC layer followed by a CNN structure, namely Reconnet is proposed to reconstruct signals directly from their compressed measurements, again obtained from a fixed random MM. The study in [22] modifies the Reconnet architecture in [21] by adding residual blocks and obtains improved performance by using the residual error between the ground truth and the preliminary reconstructed image. However, it works on image blocks, which may produce block effects in the reconstructed images. While these techniques have a common goal of learning to reconstruct an image from its compressed measurements using a neural network, the sensing matrix for all of these works are assumed to be known and in general taken as having random Gaussian entries.

In [23], an auto-encoder framework, namely DeepCodec is used to learn a transformation from the original signals to the compressed measurements allowing measurements to collect more information from the image. This is a form of dimension reduction. The measurements generated by the architecture are later used to recover the given class of signals. An extension of this work [25] is deep sparse signal representation and recovery (DeepSSRR). Both approaches learn their sensing mechanisms from the data. The method in [26] discusses adding a fully connected layer to the Reconnet architecture in [21] to learn the measurements from the given image patches. While learning sensing mechanisms from data are discussed in [25], [26], the embedding from original signal to the measurements could be nonlinear. Although nonlinear embedding could provide high performance, many applications and data acquisition systems work with linear measurements as in CS.

In this work, we propose a supervised deep learning technique with a novel architecture and loss function to jointly learn a linear MM and the sparse reconstruction scheme for a given class of signals i.e., images. Prior versions of this work with different DNN structures and analysis can be found in [27], [28]. In CS, the sensing process is linearly modelled as $\mathbf{y} = \mathbf{\Phi x}$. In this work, the MM, $\mathbf{\Phi}$, that results in the compressed measurements, $\mathbf{y}$, from the original signal, $\mathbf{x}$, is modelled as an FC network layer with linear activation functions as illustrated in Fig. 1. Hence, the linear measurement process, $\mathbf{y} = \mathbf{\Phi x}$ in classical data acquisition can be directly modelled by the weights of this FC layer that can be a part of data-driven learning.

The sparse reconstruction process in general utilizes the CS measurements and an initial starting point (proxy image) to iteratively reconstruct the image. Our goal is also to model such a process using a DNN structure. To do so the output of the first FC layer, which is generating compressed measurements, is followed by another FC layer to generate a proxy image and a set of convolutional layers with nonlinear activation functions to achieve the reconstruction of the signal in multiple stages. More detail on the selection of DNN structure is provided in Section II. The proposed end-to-end DNN learns jointly both the MM to be used to sense the signal class and a DNN structure to reconstruct images from these CS measurements. In this work, we also utilized a novel loss function. Instead of only minimizing the Euclidean loss between the input label image and the final reconstructed output image, we have also included losses between output of each reconstruction stage and the label as shown in Fig. 2, mainly to force the learning system to create enhanced mid-stage reconstructions, which also reflect in the

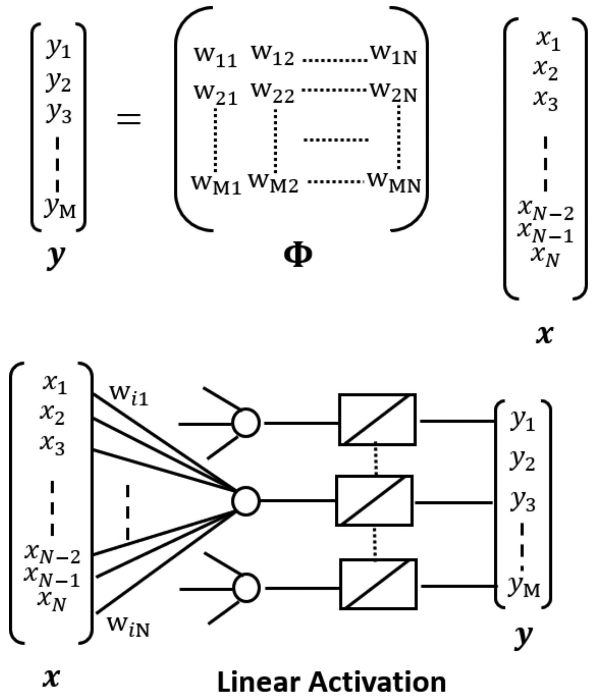

Fig. 1. (Top) Classical CS data acquisition, $\mathbf{y} = \mathbf{\Phi x}$. (Bottom) A fully connected layer with linear activation functions modeling the CS measurements in the top figure.

final reconstruction output. Use of this loss function resulted in better reconstructions as compared to minimizing the Euclidean loss between final reconstructed and true images.

The proposed structure is trained and tested on CIFAR-10 dataset [29]. The obtained results are compared with the randomly generated MMs with Gaussian entries, designed MM using (4) assuming the sparsity basis $\mathbf{\Psi}$ as the discrete cosine transform (DCT) basis, and data-driven approaches [20], [25], [26]. Results show increased performance against all compared techniques. Since the dataset contains images of various target classes, DCT is a suitable sparsity basis for the image class. The reconstruction performance is evaluated through the peak signal-to-noise ratio (PSNR) between the reconstructed and the true images and it is compared with ℓ_1 minimization based sparse recovery. Additionally, we have also incorporated the proposed DNN architecture into the generative adversarial network (GAN) [14] framework to achieve increased performance through discriminator capability. GANs mainly consist of two essential parts, namely the generator and the discriminator, both of which are DNNs themselves. However, the generator takes a set of real number in terms of a vector as the input, while, in contrast, the discriminator takes an image as the input. The aim of generator is to produce an image so that the discriminator cannot distinguish it from the real image. In this problem, the proposed DNN architecture acts as a generator, while the discriminator is created from a cascaded set of convolutional layers with a softmax layer to estimate the probability of whether the generated image is fake or not. By using such framework, we can also give rise to adversarial Euclidean loss. By using this GAN framework with the proposed form of loss, we showed that we can retain more information in terms of PSNR than that of using the proposed DNN architecture under the traditional framework with Euclidean losses.

The main contributions of this work can be stated as follows:

- A data-driven approach for learning the MM is proposed, including several new DNN structures inspired by sparse data acquisition and reconstruction techniques.
- A novel weighted multistage Euclidean error loss is utilized in the total loss function to both learn the MM and reconstruction process weights.
- A GAN framework utilizing the novel multistage end-to-end generator DNN is proposed with the adversarial loss function, resulting in enhanced reconstruction.
- Detailed performance analysis on the learned MM in comparison to the random, designed MMs and data-driven approaches are provided in terms of input image sparsity levels, number of measurements, and resulting mutual coherence levels of MMs.
- An incremental learning approach is proposed, where the system learns the next set of optimal measurements in addition to a fixed measurement set to minimize the defined cost.
- Comparisons to previously proposed DNNs in the literature and ℓ_1 minimization based techniques are provided. Learned MMs provide increased performance when they are utilized with sparse recovery with ℓ_1 minimization.

The rest of the paper is organized as follows: The proposed DNN structure is detailed in Section II. The dataset, experimental settings, and training and testing results of the proposed method with the compared techniques have been presented in Section III. Finally, conclusions are drawn in Section IV.

II. Proposed Learning Structure

The proposed multistage DNN architecture for joint learning of MM and signal reconstruction scheme is illustrated in Fig. 2. The illustrated architecture presents an end-to-end learning process, where both the measurements from an input label image and reconstructions from these compressed measurements to an output image are learned. Next, the parts of the proposed DNN structure are detailed.

A. Data Acquisition

The first part of the DNN shown in Fig. 2, including a reshaping and a fully connected layer (FC_1) models the sensing system to acquire the data from the original signal to the compressed domain i.e., the collection of the compressed linear measurements from the given class of signal. In this paper, we work on the images; hence, the input signal to the system will be $\mathbf{X} \in R^{N \times N}$. Since, the FC_1 layer is used for mapping the original signal into the linear compressed measurements; the input signal is vectorized via reshaping i.e., $\mathbf{X} \rightarrow \mathbf{x} : R^{N \times N} \rightarrow R^{N^2 \times 1}$. After reshaping, the vectorized original signal is fed into FC_1 layer to give compressed linear measurements $\mathbf{y} \in R^{M \times 1}$. This FC_1 layer models the $\mathbf{y} = \mathbf{\Phi x}$ sensing process, where entries of $\mathbf{\Phi}$ are the weights used in FC_1 layer, as illustrated in Fig. 1. In FC_1, linear activation functions are used since the data

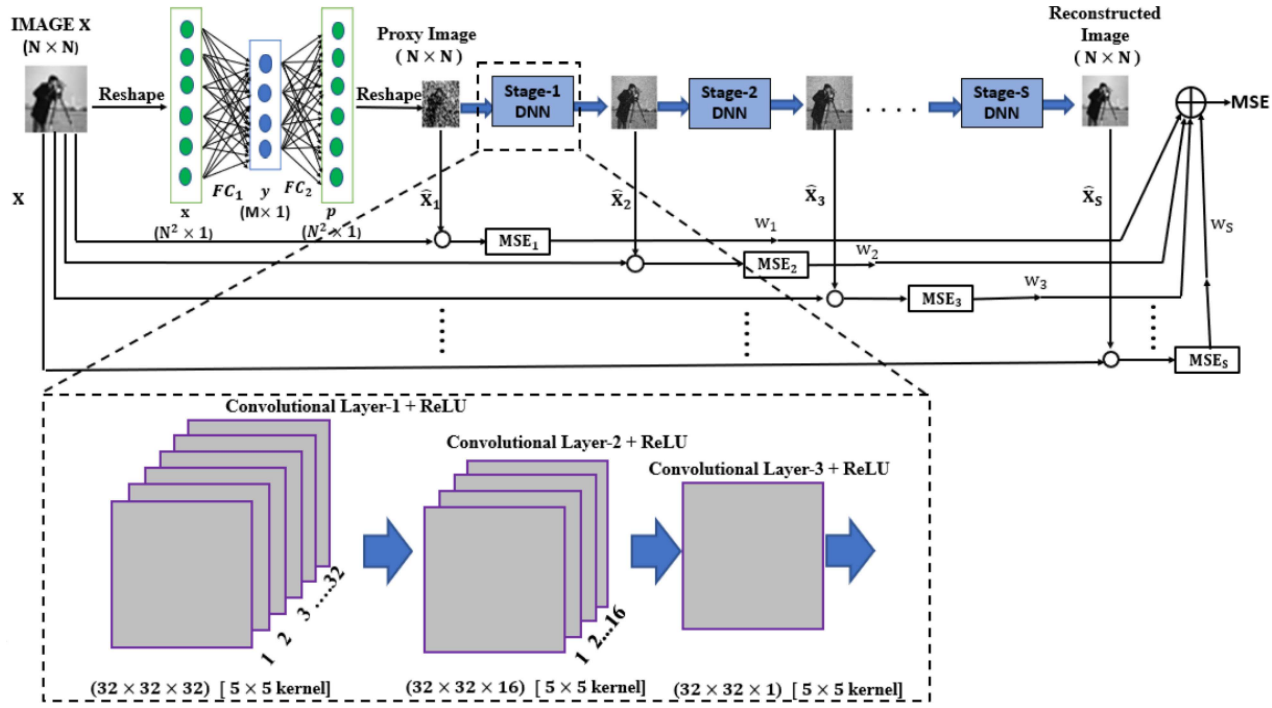

Fig. 2. Illustration of the proposed DNN structure (ConvMMNet) for joint learning of MM and sparse signal reconstruction.

acquisition process in CS systems are linear. Therefore, each measurement obtained in the compressed measurement vector $\mathbf{y}$ can be expressed as a weighted linear combination of values from $\mathbf{x}$. The dimension $(M \times N^2)$ of the weights in FC_1 also denotes the dimension of the MM.

B. Construction of the Proxy Image

Typically, sparse reconstruction approaches require an initial point to start with, such as a proxy image. The adjoint operator, $\mathbf{\Phi}^T$, normally is one way to form such a proxy output via $\mathbf{p} = \mathbf{\Phi}^T\mathbf{y}$. In the DNN structure, to create such a proxy image we have used another FC layer, which we call FC_2. The dimension of the weight in FC_2 is $(N^2 \times M)$, so that the output dimension is equal to the dimension of the input image. In our experiments, we also tested a non-trainable FC_2 to exactly model the adjoint operation $\mathbf{\Phi}^T$ using the weights of FC_1 layer; however, a trainable FC_2 layer that included nonlinear activations resulted in better performance. Hence, a trainable FC_2 is utilized in the general DNN structure. The output vector of the layer $\mathbf{p} \in R^{N^2 \times 1}$ is then reshaped to get the approximate image $\widehat{\mathbf{X}}_\mathbf{1} \in R^{N \times N}$. Next, the obtained proxy signal is fed into the reconstruction part of the architecture.

C. Multistage Signal Reconstruction

The remaining parts of the architecture following FC_2 mainly deals with the reconstruction of the image from the proxy image $\widehat{\mathbf{X}}_\mathbf{1}$. To achieve this, a series of DNN modules are used in each reconstruction stage. The final predicted output $\widehat{\mathbf{X}}_\mathbf{S}$ after passing through S stages of DNN modules is deemed as the reconstructed version of the original signal $\mathbf{X}$. The convolutional filters produces hierarchical representation of the obtained rough image to find the appropriate features that can map the estimated image closer to the true pixel values. N stages of CNNs with the same structure is utilized, where each stage uses three layers of $32, 16,$ and 1 convolutional filter, respectively. In between convolutional filters, ReLu are utilized. While a kernel size of 5×5 is used for all convolutional layers. The structure of the proposed DNN is detailed in Table-I. Previously, in [20], [27], [28], a DNN module having convolutional filters cascaded with rectified linear unit (ReLu), and average pooling (AP) layers have been used. But including average pooling layers mainly smooths the resultant image, which may be a source

TABLE I
PROPOSED DNN AND GAN NETWORK STRUCTURE

Layer Name	Input Dimension	Output Dimension	Kernel Size
Input	32× 32	-	-
FC Layer-1	1024× 1	M× 1	-
FC Layer-2	M× 1	1024× 1	-
Stage-1 DNN			
Conv.+ReLu	32 × 32× 1	32 × 32× 32	5× 5
Conv.+ReLu	32 × 32× 32	32 × 32× 16	5× 5
Conv.+ReLu	32 × 32× 16	32 × 32× 1	5× 5
Output	32 × 32× 1	-	-
Stage-2 to Stage-N DNN is same as that of Stage-1 DNN			
GAN Framework			
Generator			
Input	1024× 1	-	-
FC Layer	1024× 1	M× 1	-
Rest of the architecture is same as that of DNN structure			
Discriminator			
Input	32× 32	-	-
Conv.+ReLu	32 × 32× 1	32 × 32× 4	4× 4
Conv.+ReLu	32 × 32× 4	32 × 32× 4	4× 4
Conv.+ReLu	32 × 32× 4	32 × 32× 4	4× 4
FC Layer	4096× 1	1	-

TABLE II
AVERAGE PSNR FOR DIFFERENT SET OF TESTED MULTISTAGE WEIGHTS

w_1	w_2	w_3	M=64	M=128	M=256	M=512
0	0	1	22.24	24.32	26.74	32.79
0.075	0.075	0.85	23.15	25.41	28.49	34.51
0.15	**0.68**	**0.17**	**23.89**	**25.91**	**29.84**	**35.31**
0.25	0.25	0.5	23.49	25.74	29.60	35.02
0.33	0.33	0.34	22.68	25.07	28.28	34.37

of underfitting to the data in case of such multi-stage DNNs. Instead, in this work, in each stage, convolutional filters cascaded with only ReLu units have been used. Better reconstruction performances are obtained with excluding AP layers. Multiple stages are used to simulate the multistage approaches in sparse reconstructions. Similar approaches are also taken in DNN based approaches such as [22], [30] where each stage learns the residual error between stages. Our multistage approach together with the novel loss function provides better reconstruction performance in comparison to a single stage as shown in Table II. The classical approach is to create a loss function between the true image and final DNN output. In this case, this corresponds to a weighting of (0,0,1) for the three stage output weights (w_1, w_2, w_3) in ConvMMNet as shown in Fig. 2. The hypothesis we wanted to test was whether forcing the intermediate stage outputs of ConvMMNet to be closer to the true image by adding a weighted share from their loss to the total loss would help the final image reconstruction performance. To test this hypothesis, we simulated a set of weights; from not including intermediate stage outputs at all to equally weighting all stage outputs. It can be seen that using a learned weight combination of $(w_1 = 0.15, w_2 = 0.68, w_3 = 0.17)$ resulted the highest PSNR levels for all tested number of measurements. This weight combination also provides approximately 3 dB higher PSNR compared to the case where only end-to-end loss term is considered. Performance change with number of stages is discussed in Section III.

The goal of the DNN is to reconstruct an image that is as close to the ground truth image $\mathbf{X}$ as possible in mean squared sense. However, the proposed multistage DNN provides the additional advantage by producing intermediate image outputs, which are then used in the calculation of the loss to be minimized. To force the DNN to create better intermediate images, and through that a better final output, we propose to use a weighted mean squared loss as

$$L_W(\Theta) = \frac{1}{T}\sum_{i=1}^{T}\left(\sum_{k=1}^{S} w_k \|\widehat{\mathbf{X}}_{k,i}(\Theta) - \mathbf{X_i}\|_F\right). \quad (5)$$

The total weighted loss $L_W(\Theta)$ in (5) is calculated over the the total number of T training samples and it is backpropagated to optimize the weights in the associated convolutional and FC layers to minimize $L_W(\Theta)$. The reconstructed image $\widehat{\mathbf{X}}_{k,i}$ is a function of the learned parameters Θ and the weights w_k represents the importance of the loss for the corresponding stage k. In this work, instead of making the w_k as hyperparameter, we have also make it learnable so that set of weights that produce the most optimum intermediate reconstruction of the images can be obtained. Model based reconstruction approaches such as [31] have utilized data consistency layers, which effectively requires outputs of stages to be close to the measurements through unrolling the classical sparsity constraint optimization algorithms. Data consistency layers in [31] use proxy conjugate gradient steps in an iterative fashion to recover sparse signals. The presented weighted loss function also provides a similar consistency effect through forcing intermediate stage outputs to be closer to the true data sample along with learning the weights used after each stage from data. Our results showed that using a properly weighted total loss produces enhanced reconstructions in average compared to only minimizing the loss between the final output and true images. This process creates a learned DNN structure, where the first fully connected layer FC_1 will correspond to the learned linear MM to sense the class of signal. The remaining layers of the DNN take compressed measurements and output the reconstructed image. The overall structure of the proposed DNN is shown in Fig. 2 and is henceforth referred to as 'ConvMMNet' throughout the remainder of the paper.

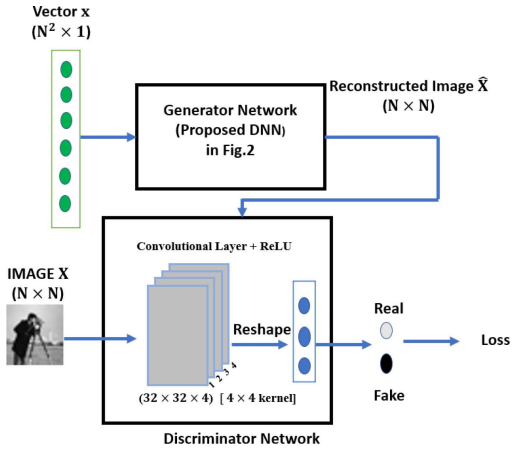

Fig. 3. Block diagram of the GAN using the proposed DNN as generator.

D. Multistage Signal Reconstruction in Adversarial Framework

In addition to the multistage DNN shown in Fig. 2, we have also used the adversarial losses in tandem with the multistage Euclidean loss to learn both the MM and the reconstruction network. For the adversarial loss, we have modified the loss function by introducing the proposed DNN into the GAN framework shown in Fig. 3. The GAN is comprised of two networks: the generator, and the discriminator. The generator network $G(.)$ accepts as input the vector $\mathbf{x} \in R^{N^2\times 1}$, which is the vectorized version of the input image $\mathbf{X} \in R^{N\times N}$ and then uses the proposed ConvMMNet architecture to estimate the reconstructed image $\hat{\mathbf{X}}$. Then, this estimated reconstruction, along with the original image, $\mathbf{X}$ is passed to the discriminator network $D(.)$ to classify whether the obtained image is real or fake. The main motivation here is to improve the performance of the generator network such that the reconstructed image can fool the original image, which is fed into the discriminator network. The discriminator network $D(.)$ takes a two dimensional signal of size $N \times N$ as its input. It has a CNN structure with a kernel

size of 4×4 in each layer with ReLu activations. Then, the output of the CNN stage is reshaped into a vector, which is fed into a FC layer with a dropout rate of 0.5 to get the classification accuracy that corresponds to the probability of the output image being real or fake.

The loss term in the discriminator of the GAN measures how well it can classify the true image (real) and the reconstructed images (fake) generated by the ConvMMNet model, and may be expressed as,

$$L_D = \frac{1}{T}\sum_{i=1}^{T} L_{CE}(D(\mathbf{X_i}), 1) + L_{CE}(D(G(\mathbf{x_i})), 0), \quad (6)$$

where L_{CE} denotes the cross entropy calculated for both real and fake images with ground truth labels being assigned to one and zero respectively. L_{CE} is expressed in (7) as

$$L_{CE}(\hat{z}, z) = -z log\hat{z} + (1-z) log(1-\hat{z}). \quad (7)$$

The generator loss L_G is defined as the combination of Euclidean loss in (5) and adversarial loss in (6). Therefore, the total loss in the generator network can be expressed as

$$L_G(\Theta_D, \Theta_G) = \frac{\lambda_G}{T} L_W(\Theta_G) + \frac{\lambda_D}{T} \times \sum_{i=1}^{T} L_{CE}(D(G(\mathbf{x}_i, \Theta_G), \Theta_D), 1). \quad (8)$$

The hyperparameters λ_G, λ_D are selected to be 1 and 0.0001, respectively in order to regularize the parameters from the generator and the discriminator networks. The learning rate for both G and D has been set as 10^{-4}. The update Θ_G is done at twice the rate of Θ_D because the discriminator converges much faster than the generator [14]. In this way, we can update the parameters via the combination of Euclidean and adversarial loss functions. This adversarial framework is shown in Fig. 3 and is referred to as 'ConvMMNet-GAN' in the remainder of the paper. Details on its structure are provided in Table I.

III. Simulation Results

A. Experimental Settings

For training, validating, and testing of the proposed end-to-end DNN structures utilizing joint learning of the MM and image reconstruction as described in Section II, we have exploited the publicly available dataset, CIFAR-10 [29]. This dataset is widely exploited for computer vision tasks like object detection and classification [32]. It contains a total of 60000 color images of size $32 \times 32 \times 3$ from ten different object classes. Since our main goal is image reconstruction rather than classification; we only use image class information to design the train and test datasets. For the simulations. two different train/validation/test dataset setups are developed. In the first case, which we call Training-1, the whole dataset is split into six batches, where five of them are used for training and validating and remaining one is used for testing. Test set consists of 10000 images, mainly 1000 examples from each of the ten objects. The remaining set is shuffled so that number of examples are varying in each batch and 80% of them are used for training and 20% of them are used for validation. Hence in Training-1 40000 images are used for training, 10000 for validation, and 10000 for testing. In the second configuration (Training-2), we have excluded all images of one object class from the training and used these samples as test dataset where training dataset is formed using samples from all object classes except the excluded one. Hence, in this case, we have 6000 test set images from one single object class and 54000 of images from all other object classes. 80% images out of 54000 have been used for training and rest of them are used as validation data. The color images in the dataset are converted to grayscale and all learning and simulations are done on grayscale images. For evaluating the reconstruction performance of the proposed DNN structures we opt to use the peak to signal noise ratio (PSNR) [33] metric defined as,

$$PSNR = 10\log_{10}\frac{\max_{\mathbf{X}}^2}{\|\mathbf{X} - \widehat{\mathbf{X}}_\mathbf{i}\|_2^2} \quad (9)$$

where, $\max_{\mathbf{X}}$ is the maximum intensity value of the given image $\mathbf{X}$.

The backpropagation of the proposed DNNs is done by using a mini-batch gradient descent routine. To accelerate correct learning process we split the dataset into a set of batches. We have set the mini-batch size to 32 for our simulations and run the backpropagation for 500 epochs with an exponentially decaying learning rate from 0.1 to 0.0001 to find the optimized parameters to reconstruct the final image. We have used Tensorflow [34], the open source deep learning framework, in this work for training and testing purposes.

B. Simulations on the Design of ConvMMNet Structure

To achieve the DNN architectures presented in Section II, several simulations are carried out both to evaluate the performance and determine the choice of structure to be used in the final DNN. In all simulations to determine the structure of the network, only validation datasets are used. Test datasets are only used for the final network. In Fig. 2, the second fully connected layer (FC_2) is designed to create an initial rough image. In sparse reconstruction, an initial starting point could be constructed through the adjoint operator as $\widehat{\mathbf{x}} = \mathbf{\Phi}^T\mathbf{y}$ where $\mathbf{\Phi}$ is the MM. We first tested on a non-trainable FC_2 with weights obtained as transpose of FC_1 weights, and compared this with a trainable FC layer. We observed that a trainable FC_2 layer was resulting in 0.9 dB more average PSNR performance as compared to the former case. Hence a trainable FC_2 layer is used in the final architecture. In terms of initialization of DNN weights, all layers are initialized with randomly selected weights. We tested initializing the FC_1 layer with the weights obtained from the designed MM for the DCT basis. We observed that the resultant difference between initializing FC_1 randomly and using designed weights was less than 0.3 dB, hence we selected random initialization to keep it more general. Another test is done on the number of stages used in the reconstruction part of the DNN. Compared to a single stage system as presented in our initial study [27], using multiple reconstruction stages improved

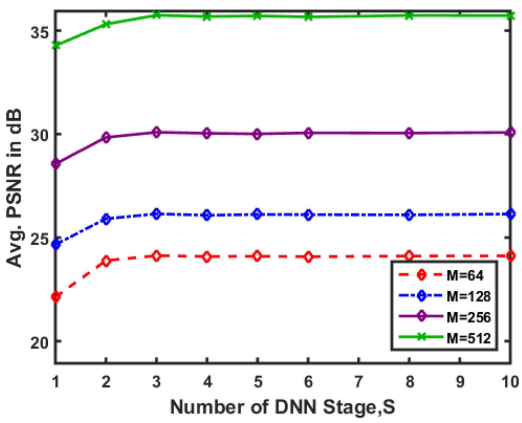

Fig. 4. Testing performance as a function of different number of DNN stages.

the average PSNR results approximately 2 dB. However, using more stages may only result in almost the same reconstruction performance on the validation data. The fact is evident in Fig. 4. It is seen that using more than three stages the average PSNR didn't bring further performance increase and hence a three stage system is used in the final DNN architecture.

C. Compared Approaches and Qualitative Results

To analyze the performance of the learned MM and the reconstruction networks, we have compared the proposed approaches with other MMs and recovery techniques. The learned MMs from ConvMMNet and ConvMMNet-GAN structures are compared with random MM with entries selected from the standard normal distribution and designed MM as described in [9] assuming DCT as the sparsity basis, adaptive or learned MMs as obtained from using DeepSSRR [25], learned Reconnet and its GAN version [26]. These MMs are utilized in both DNN based reconstructions and constraint ℓ_1 minimization based sparse recovery. In ℓ_1 minimization, sparsity basis is used as the DCT basis. For DNN based reconstruction, two proposed networks in this work are also compared with DeepInverse (DI) [20] and original Reconnet [21] approaches, where both networks use compressed measurements from random MM as their inputs. In [21], [26], [30], mainly a 33×33 overlapping blocks are used to represent the image. Here, instead we have used 32×32 images from the CIFAR-10 dataset to reimplement the DNN architecture in [21], [26], [30]. In these comparisons, the goal is to understand the effectiveness of MMs in terms of signal recovery under different recovery approaches and to compare DNN and ℓ_1 minimization based techniques under the same framework. Although there are many other sparse recovery approaches [5], [35]–[37], their performance compared to ℓ_1-recovery is well established. Hence comparison of the performance of learned MMs with other sparse recovery techniques is not discussed in this paper. However, the learned MMs and the resultant compressed measurements can be used with any sparse recovery technique to achieve an enhanced result. The reconstruction result for an example test set image is shown in Fig. 5 for all compared approaches along with the obtained PSNR values. All compared approaches use 256 measurements for this 32×32 image. The highest PSNR for this qualitative analysis is obtained by the learned MM obtained via the proposed ConvMMNet-GAN. While ℓ_1-recovery performs comparably better than some DNN reconstructions for random MM cases, the joint learning of MM and DNN reconstruction achieves better reconstruction performance as classical CS recovery scenario of random MM and ℓ_1-recovery. The images shown in Fig. 5 are results on a single example image. Next subsections provide more quantitative analysis on average performances over the full test dataset as a function of number of measurements, incremental measurement designs, effect of signal sparsity on DNN based reconstructions, and coherence analysis on the learned MMs.

D. Quantitative Analysis

For quantitative evaluation, all the DNN architectures are run over the testing dataset, for varying number of compressed measurements from $M = 64$ to $M = 512$. After obtaining the outputs, the reconstruction performance of compared techniques are evaluated in terms of the PSNR metric. The average, maximum and minimum PSNRs obtained over the test dataset have been reported on Table III and the average PSNRs are illustrated in Fig. 6. From both visual and quantitative perspectives, it can be seen that for all the measurement cases, the proposed ConvMMNet-GAN architecture produces the best MM resulting the highest PSNR levels. The learned MMs by the proposed architectures outperform the randomly created and designed MMs by around $6-16$ dB in PSNR levels when it is used in DNN based reconstruction, or $3-7$ dB when employed in ℓ_1-based recovery. In addition, the designed MM that is defined as optimal in the sense of minimizing average mutual coherence for the given sparsity basis is not optimal in terms of average reconstruction performance and the learned MM from ConvMMNet-GAN provides $6-13$ dB more PSNR than this designed MM. In addition, we also see that both ConvMMNet and ConvMMNet-GAN structures outperform the concurrent state-of-the-art learned MMs (Reconnet and its gan version, DeepSSRR, and ISTANET) by having $1-5$ dB more average PSNR than them. Moreover, DNN based reconstruction with learned MMs outperform ℓ_1 based reconstruction, when these learned MMs are utilised in ℓ_1 recovery indicating the supremacy of data driven reconstruction. However, in case of ℓ_1 based reconstruction, the MMs learned through proposed ConvMMNet and ConvMMNet-GAN outperform all compared MM cases by having $1-2$ dB more PSNR. It is also seen that the learned MM by the ConvMMNet-GAN results around 1 dB higher PSNR than ConvMMNet.

E. Incremental Measurement Design Results

The proposed ConvMMNet learns the MM for a fixed given number of measurements, M. While MMs can be learned independently for different number of measurements, another way is incremental learning. In this incremental learning approach, given a fixed number of measurements M_0, we learn the next ΔM number of measurements to have a total of $M = M_0 + \Delta M$ measurements. In this approach, while the weights on FC_1 that corresponds to the initial M measurements are

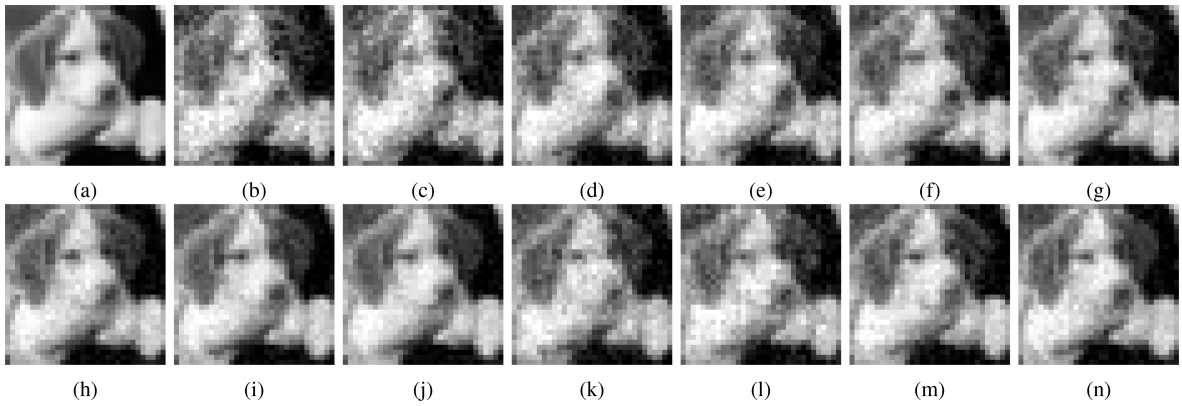

Fig. 5. Reconstructed images for the learned, fixed and designed MMs for 256 measurements. PSNRs are shown in parentheses. (a) Original Image, (b) Φ_R-DI (21.16 dB), (c) Φ_D-DI (21.52 dB), (d) Φ_R-Reconnet (23.56 dB), (e) Φ_L-DeepSSRR (24.70 dB) (f) Φ_L-Reconnet (25.12 dB), (g) Φ_L-Reconnet-GAN (26.43 dB), (hISTANET$^+$ (28.43 dB), (i) Φ_L-ConvMMNet (29.60 dB), (j) Φ_L-ConvMMNet-GAN (29.93 dB), (k) Φ_R+ℓ_1 (23.80 dB), (l) Φ_D+ℓ_1 (24.54 dB), (m) Φ_L-ConvMMNet +ℓ_1 (26.50 dB), (n) Φ_L-ConvMMNet-GAN + ℓ_1 (27.62 dB).

TABLE III
COMPARISON FOR DIFFERENT METHODS TO RECONSTRUCT IMAGES WITH DIFFERENT NUMBER OF MEASUREMENTS

Method	Meas. No	DNN Based recovery (PSNR-dB)			ℓ_1 Based recovery (PSNR-dB)		
		Average	Minimum	Maximum	Average	Minimum	Maximum
$\mathbf{\Phi}_R$ DI	64	18.12	10.51	25.92	21.08	14.46	25.89
$\mathbf{\Phi}_D$ DI		18.23	10.73	26.08	21.19	14.63	26.16
$\mathbf{\Phi}_R$ Reconnet		21.09	13.18	28.06	21.08	14.46	25.89
$\mathbf{\Phi}_L$ DeepSSRR		21.75	14.46	29.78	21.61	14.44	29.69
$\mathbf{\Phi}_L$ Reconnet		22.08	14.38	30.16	21.96	14.21	30.02
$\mathbf{\Phi}_L$ Reconnet-GAN		22.81	15.28	31.25	22.93	15.32	31.17
ISTANET$^+$		23.67	16.37	32.03	21.08	14.46	25.89
$\mathbf{\Phi}_L$ ConvMMNet		24.13	16.29	32.13	23.52	15.18	31.18
$\mathbf{\Phi}_L$ ConvMMNet-GAN		**24.34**	**16.41**	**32.26**	**23.60**	**15.26**	**31.28**
$\mathbf{\Phi}_R$ DI	128	19.37	11.31	26.67	21.84	15.71	29.02
$\mathbf{\Phi}_D$ DI		19.51	11.43	26.99	21.98	15.83	29.21
$\mathbf{\Phi}_R$ Reconnet		22.81	13.47	29.93	21.84	15.71	29.02
$\mathbf{\Phi}_L$ DeepSSRR		23.34	15.29	30.89	22.86	14.81	30.02
$\mathbf{\Phi}_L$ Reconnet		23.89	15.38	31.16	22.91	14.98	30.18
$\mathbf{\Phi}_L$ Reconnet-GAN		24.96	16.54	32.13	24.05	16.02	31.24
ISTANET$^+$		25.61	17.43	33.16	21.84	15.71	29.02
$\mathbf{\Phi}_L$ ConvMMNet		26.15	18.08	34.31	25.05	16.43	32.19
$\mathbf{\Phi}_L$ ConvMMNet-GAN		**27.19**	**17.73**	**33.79**	**25.29**	**16.81**	**32.41**
$\mathbf{\Phi}_R$ DI	256	19.98	11.92	29.17	22.57	18.06	31.53
$\mathbf{\Phi}_D$ DI		20.84	11.94	29.26	22.61	18.35	31.46
$\mathbf{\Phi}_R$ Reconnet		24.12	14.02	31.48	22.57	18.06	31.53
$\mathbf{\Phi}_L$ DeepSSRR		26.02	16.61	33.89	25.92	21.49	35.42
$\mathbf{\Phi}_L$ Reconnet		26.28	15.84	34.17	26.03	21.71	35.81
$\mathbf{\Phi}_L$ Reconnet-GAN		28.08	17.08	35.23	27.75	22.46	36.02
ISTANET$^+$		29.12	18.42	36.86	22.57	18.06	31.53
$\mathbf{\Phi}_L$ ConvMMNet		30.09	20.18	38.46	29.81	19.65	36.12
$\mathbf{\Phi}_L$ ConvMMNet-GAN		**31.06**	**20.67**	**38.73**	**29.94**	**20.01**	**36.24**
$\mathbf{\Phi}_R$ DI	512	20.92	12.34	30.01	23.05	17.31	32.19
$\mathbf{\Phi}_D$ DI		21.84	12.58	30.94	24.18	18.70	32.43
$\mathbf{\Phi}_R$ Reconnet		25.66	14.38	32.97	23.05	17.31	32.19
$\mathbf{\Phi}_L$ DeepSSRR		29.93	17.65	35.19	28.44	22.31	36.23
$\mathbf{\Phi}_L$ Reconnet		32.08	18.65	37.63	29.16	22.89	37.45
$\mathbf{\Phi}_L$ Reconnet-GAN		33.28	20.02	38.97	30.02	23.63	38.52
ISTANET$^+$		34.42	21.27	41.16	23.05	17.31	32.19
$\mathbf{\Phi}_L$ ConvMMNet		35.74	21.02	42.03	30.41	19.67	37.08
$\mathbf{\Phi}_L$ ConvMMNet-GAN		**36.08**	**21.97**	**42.87**	**30.93**	**24.08**	**37.76**

fixed, learning is done only on the weights corresponding to the next ΔM measurements. In Fig. 7, we compare the performance of the incrementally learned MM with directly learning the full M measurements within ConvMMNet, and also random and designed MMs. Although the incremental learning performs slightly less than the learning MMs directly, the performance difference is less than 0.7 dB in PSNR at all measurements. It can also be seen that the incrementally learned MMs still provide approximately 7 dB higher PSNR compared to random or designed MMs.

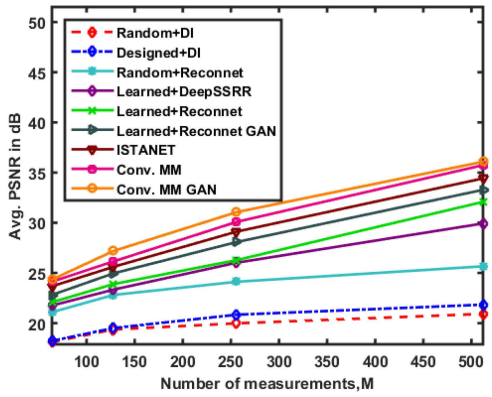

(a)

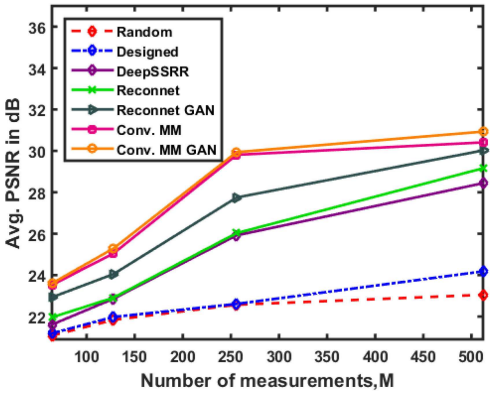

(b)

Fig. 6. Avg. PSNR as a function of number of measurements (a) for DNN based compared techniques, (b) when varying random, designed or learned MMs are utilized in ℓ_1 recovery.

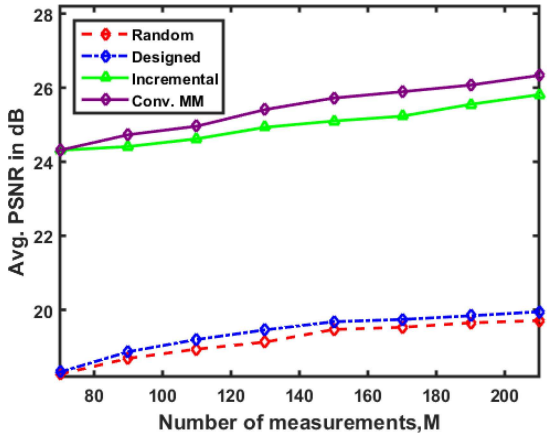

Fig. 7. Avg. PSNR as a function of number of measurements for the directly learned, incrementally learned, random, and designed MMs used in DNN based reconstruction.

F. Out of Class Training Results

The DNN based reconstruction results presented in previous subsections were trained using 'Training set-1' where examples of all input target classes are available in training and validation datasets. To analyze the effect of target class dependence on reconstruction performance, we have tested the performance of the learned DNN structures using a 'Training set-2'. In this training set, 9 out of the total of 10 target class samples are used in the training and the learned ConvMMNet is tested to reconstruct the images for the left out target class. The reconstruction of an example test image using compared techniques is shown in Fig. 8 for $M = 256$ measurements. It can be seen that the best reconstruction is obtained using the learned MM by the proposed ConvMMNet-GAN. Fig. 9 shows the average PSNR comparison between the two mentioned train/test cases. It is seen that although there is approximately 0.6 dB performance difference between the two training approaches, both cases perform similarly as number of measurements increases. This slight difference between two training approaches are due to the fact that 'Training-1' has examples from all target classes, while 'Training-2' has no similar object class in the training dataset. We expect that this difference will even be smaller in a larger dataset as number of target classes in the training sets increases.

G. Effect of Sparsity in DNN Based Reconstruction

The complexity of the images is an important parameter for the assessment of DNNs to learn reconstructing them. Can DNN reconstruct a simpler image better than a more complex one? To analyze the learning capability of the proposed DNN architectures as the complexity of the underlying signals change, a simulation is developed. We model the signal complexity with the sparsity level of the signals. The full CIFAR-10 dataset is regenerated with varying sparsity levels from $K = 5$ to $K = 400$, using DCT as the sparsity basis. For each level of sparsity, ConvMMNet is trained, validated, and tested on the corresponding sparse CIFAR-10 dataset. The obtained average PSNR reconstruction performance as a function of sparsity level is shown in Fig. 10. It can be seen that ConvMMNet learns to reconstruct higher PSNR images with increasing measurements for the same sparsity levels. For a given number of measurement, it reconstructs sparser images better which reflects that simpler images can be reconstructed easier compared to more complex images. It is also important to note that after some sparsity level PSNR values are approximately flat. This shows that at a given measurement number M ConvMMNet can reconstruct up to a maximum level of sparsity level K, which increases by M, similar to sparse reconstruction approaches. In addition, the learned MMs from these simulations are utilized in ℓ_1 based recovery and compared with the random MMs. Note that the random MM with ℓ_1 based recovery is the classical CS approach. Fig. 11 shows the transition curves at compared sparsity levels as a function of number of measurements M. It can be seen that the learned MMs achieve the transition at lower M values for all tested sparsity levels compared to the random MMs.

H. Analysis on the Learned MM

The mutual coherence and the selected sparsity basis are important parameters that effect the signal reconstruction performance as defined in (1). The proposed DNN structure does not assume a sparsity basis nor specifically tries to minimize

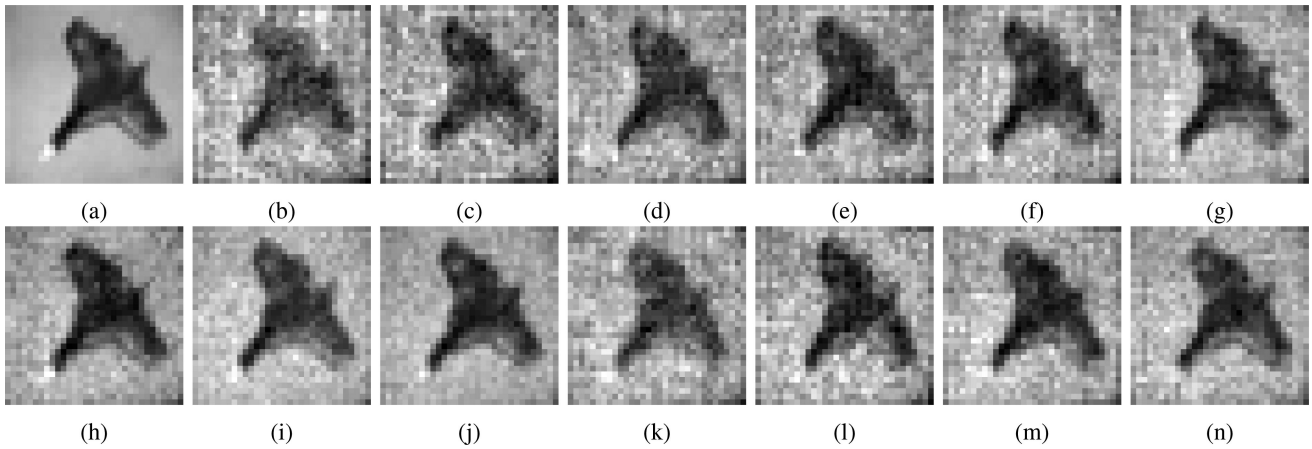

Fig. 8. Reconstructed images for the learned, fixed and optimal sensing matrix for 256 measurements using samples from class that is not used for training (a) Original Image, (b) Φ_R-DI (23.59 dB), (c) Φ_D-DI (24.29 dB), (d) Φ_R-Reconnet (26.27 dB), (e) Φ_L-DeepSSRR (26.51 dB), (f) Φ_L-Reconnet (27.78 dB), (g) Φ_L-Reconnet-GAN (29.02 dB), (h) ISTANET$^+$ (30.47 dB), (i) Φ_L-ConvMMNet (31.68 dB), (j) Φ_L-ConvMMNet-GAN (32.79 dB), (k) $\Phi_R + \ell_1$ (26.09 dB), (l) $\Phi_D + \ell_1$ (26.80 dB), (m) Φ_L-ConvMMNet + ℓ_1 (28.52 dB), (n) Φ_L-ConvMMNet-GAN + ℓ_1 (29.30 dB).

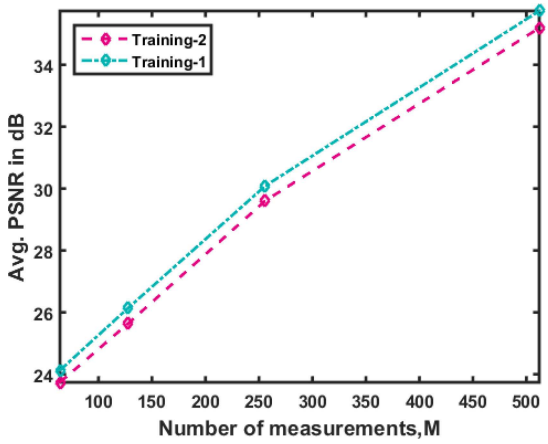

Fig. 9. Avg. PSNR as a function of number of measurements for Training-1 and Training-2 cases.

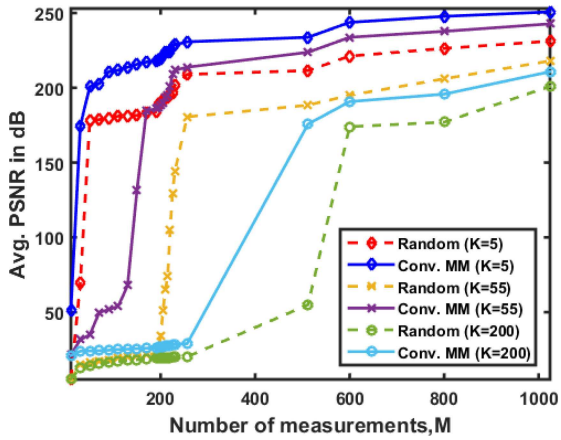

Fig. 11. Transition curves at different different sparsity levels ($K = 5$, $K = 55$, and $K = 200$) as a function of number of measurements.

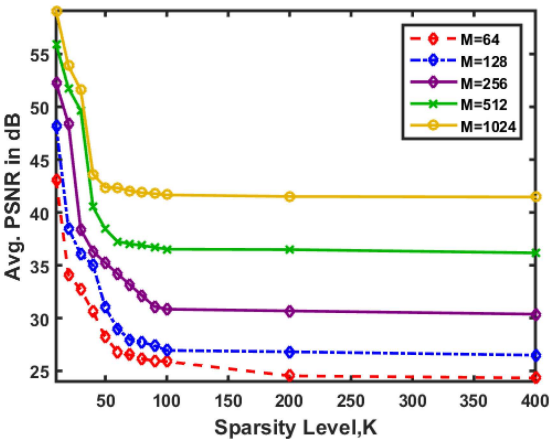

Fig. 10. Average PSNR for different measurement numbers M as a function of sparsity level K.

a parameter like mutual coherence. Nevertheless, we made a simulation to understand the coherence properties of the learned MMs. The sparsity basis $\mathbf{\Psi}$ is assumed to be DCT basis and the mutual coherence of the system $\mathbf{A} = \mathbf{\Phi}\mathbf{\Psi}$ is calculated for the MM $\mathbf{\Phi}$. We tested random MM, learned MMs for ConvMMNet, DeepSSRR, Reconnet, and the designed MM for the assumed basis. We show the average mutual coherence as a function of number of measurements in Fig. 12. It can be seen that the designed MM has the lowest average coherence since it is designed specifically for that purpose. The learned MMs have more average coherence compared to random MMs. On the other hand, it can be seen from the histogram plots of the coherence shown in Fig. 13 that the designed MM almost has the highest maximum absolute coherence while learned MMs from ConvMMNet and Reconnet have similar values with that of designed one. On the contrary, learned MM in DeepSSRR and random MM have similar lower values of absolute coherence. Presented results in this paper show that the learned MM provides the

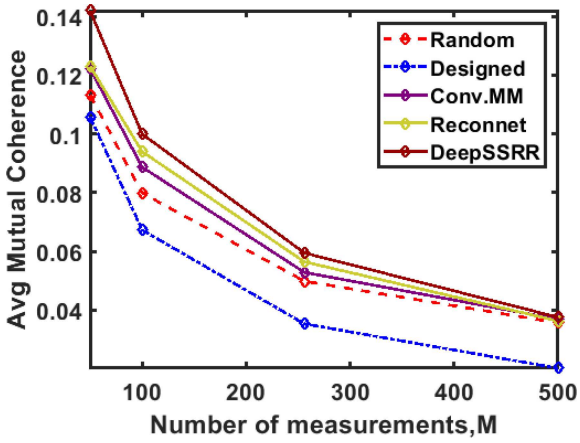

Fig. 12. Average mutual coherence of the tested learned, designed and random MMs with the DCT basis as a function of number of measurements M.

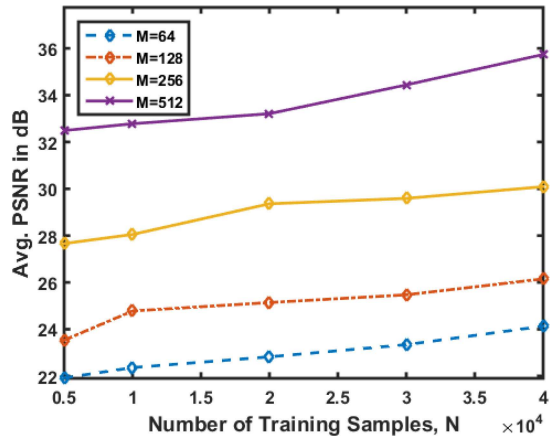

Fig. 14. Avgr. PSNR in dB with respect to the increasing number of training samples.

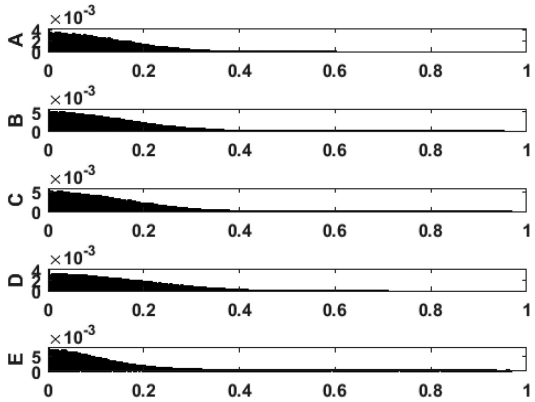

Fig. 13. Histogram for the coherence values of tested MMs at $M = 128$, [A: Random, B: ConvMMNet, C: Reconnet, D: DeepSSRR, E: Designed].

best reconstruction performance of compared MMs although not necessarily minimizing average or absolute coherence values. We think that this is because first average mutual coherence is not directly guarantee better reconstruction performance and secondly the assumed DCT basis may not be the best basis for the tested image dataset.

I. Performance as a Function of Training Set Size

The number of training samples for proposed DNNs for learning to reconstruct images is an important parameter. CIFAR-10 dataset has a total of 60000 images and 'Training-1' case used 40000 images as the training set, 10000 images as the validation set for learning. To analyze the reconstruction performance of the ConvMMNet as a function of the increasing number of training samples we changed the training set size from 5000 to 40000 while still testing the learned network on the same test dataset. The obtained average PSNR result is shown in Fig. 14. It can be seen that as the DNN uses more training samples for learning, its image reconstruction performance on the test dataset increases. Due to the small size of CIFAR-10, it is not clear if or at what training sample size this performance converges to a level. Our expectation is that by increasing the training set size utilizing a larger dataset, the DNN reconstruction has the potential to increase its performance.

IV. Conclusion

In this work, we propose a deep neural network (DNN) structure with cascaded fully connected and convolutional layers utilizing a multilevel trainable weighted loss function in an adversarial learning framework to learn both the measurement matrix (MM) and the inverse reconstruction scheme for images. The proposed networks are trained,validated, and tested on CIFAR-10 database and compared with random MM with Gaussian entries, designed, and adaptive MMs to minimize the average coherence with the DCT basis. Learned MMs are also utilized in ℓ_1 minimization based sparse recovery.Learned MMs through proposed approach provide higher PSNR over the test dataset than the compared MMs in both DNN or ℓ_1 based reconstructions. The proposed approach also provides incremental measurement learning where the system can learn the next set of measurements on top of a fixed set of measurements. More training samples help networks learn better reconstruction schemes. Different training scenarios showed that the reconstructions don't depend on the object classes in the dataset. The effect of sparsity levels of the underlying images on the reconstruction performance of the learned networks is also studied. It is observed that learned networks could reconstruct sparser images with higher PSNR and performance increasing with the number of measurements. The proposed reconstruction scheme has less computational complexity compared to ℓ_1 minimization based reconstructions with superior results. While provided MM learning focus on linear sensing systems, learning nonlinear sensing mechanisms from data can also be a future research topic.

References

[1] E. Candès, J. Romberg, and T. Tao, "Stable signal recovery from incomplete and inaccurate measurements," *Commun. Pure Appl. Math.*, vol. 59, no. 8, pp. 1207–1223, 2006.
[2] E. J. Candès and M. B. Wakin, "An introduction to compressive sampling," *IEEE Signal Process. Mag.*, vol. 25, no. 2, pp. 21–30, Mar. 2008.

[3] D. L. Donoho, A. Maleki, and A. Montanari, "Message-passing algorithms for compressed sensing," *Proc. Nat. Acad. Sci.*, vol. 106, no. 45, pp. 18914–18919, 2009.
[4] J. Tropp, "Greed is good: Algorithmic results for sparse approximation," *IEEE Trans. Inf. Theory*, vol. 50, no. 10, pp. 2231–2242, Oct. 2004.
[5] J. A. Tropp and A. C. Gilbert, "Signal recovery from random measurements via orthogonal matching pursuit," *IEEE Trans. Inf. Theory*, vol. 53, no. 12, pp. 4655–4666, Dec. 2007.
[6] C. Hegde, A. C. Sankaranarayanan, W. Yin, and R. G. Baraniuk, "Numax: A convex approach for learning near-isometric linear embeddings," *IEEE Trans. Signal Process.*, vol. 63, no. 22, pp. 6109–6121, Nov. 2015.
[7] M. Elad, "Optimized projections for compressed sensing," *IEEE Trans. Signal Process.*, vol. 55, no. 12, pp. 5695–5702, Dec. 2007.
[8] J. M. Duarte-Carvajalino and G. Sapiro, "Learning to sense sparse signals: Simultaneous sensing matrix and sparsifying dictionary optimization," *IEEE Trans. Image Process.*, vol. 18, no. 7, pp. 1395–1408, Jul. 2009.
[9] L. Zelnik-Manor, K. Rosenblum, and Y. C. Eldar, "Sensing matrix optimization for block-sparse decoding," *IEEE Trans. Signal Process.*, vol. 59, no. 9, pp. 4300–4312, Sep. 2011.
[10] G. Li, Z. Zhu, D. Yang, L. Chang, and H. Bai, "On projection matrix optimization for compressive sensing systems," *IEEE Trans. Signal Process.*, vol. 61, no. 11, pp. 2887–2898, Jun. 2013.
[11] Y. LeCun, Y. Bengio, and G. Hinton, "Deep learning," *Nature*, vol. 521, no. 7553, pp. 436–444, 2015.
[12] A. Krizhevsky, I. Sutskever, and G. E. Hinton, "Imagenet classification with deep convolutional neural networks," in *Proc. Adv. Neural Inf. Process. Syst.*, 2012, pp. 1097–1105.
[13] P. Vincent, H. Larochelle, I. Lajoie, Y. Bengio, and P.-A. Manzagol, "Stacked denoising autoencoders: Learning useful representations in a deep network with a local denoising criterion," *J. Mach. Learn. Res.*, vol. 11, pp. 3371–3408, 2010.
[14] I. Goodfellow *et al.*, "Generative adversarial nets," in *Proc. Adv. Neural Inf. Process. Syst.*, 2014, pp. 2672–2680.
[15] F. N. Iandola, S. Han, M. W. Moskewicz, K. Ashraf, W. J. Dally, and K. Keutzer, "Squeezenet: Alexnet-level accuracy with 50x fewer parameters and $<$ 0.5 mb model size," 2016, *arXiv:1602.07360*.
[16] S. Zagoruyko and N. Komodakis, "Wide residual networks," 2016, *arXiv:1605.07146*.
[17] K. Simonyan and A. Zisserman, "Very deep convolutional networks for large-scale image recognition," in *3rd Int. Conf. Learn. Representations*, 2015.
[18] A. Lucas, M. Iliadis, R. Molina, and A. K. Katsaggelos, "Using deep neural networks for inverse problems in imaging: Beyond analytical methods," *IEEE Signal Process. Mag.*, vol. 35, no. 1, pp. 20–36, Jan. 2018.
[19] A. Mousavi, A. B. Patel, and R. G. Baraniuk, "A deep learning approach to structured signal recovery," in *Proc. IEEE 53rd Annu. Allerton Conf. Commun., Control, Comput. (Allerton)*, 2015, pp. 1336–1343.
[20] A. Mousavi and R. G. Baraniuk, "Learning to invert: Signal recovery via deep convolutional networks," in *Proc. IEEE Int. Conf. Acoust., Speech, Signal Process.*, 2017, pp. 2272–2276.
[21] K. Kulkarni, S. Lohit, P. Turaga, R. Kerviche, and A. Ashok, "Reconnet: Non-iterative reconstruction of images from compressively sensed measurements," in *Proceedings IEEE Conf. Comput. Vision Pattern Recognit.*, 2016, pp. 449–458.
[22] H. Yao *et al.*, "Dr2-net: Deep residual reconstruction network for image compressive sensing," *Neurocomputing*, vol. 359, pp. 483–493, 2019.
[23] A. Mousavi, G. Dasarathy, and R. G. Baraniuk, "Deepcodec: Adaptive sensing and recovery via deep convolutional neural networks," 2017, *arXiv:1707.03386*.
[24] X. Xie, Y. Wang, G. Shi, C. Wang, J. Du, and X. Han, "Adaptive measurement network for cs image reconstruction," in *Proc. CCF Chin. Conf. Comput. Vision*, 2017, pp. 407–417.
[25] A. Mousavi, G. Dasarathy, and R. G. Baraniuk, "A data-driven and distributed approach to sparse signal representation and recovery," in *Proc. Int. Conf. Learn. Representations*, 2019.
[26] S. Lohit, K. Kulkarni, R. Kerviche, P. Turaga, and A. Ashok, "Convolutional neural networks for noniterative reconstruction of compressively sensed images," *IEEE Trans. Comput. Imag.*, vol. 4, no. 3, pp. 326–340, Sep. 2018.
[27] R. MdRafi and A. C. Gurbuz, "Learning to sense and reconstruct a class of signals," in *Proc. IEEE Radar Conf.*, Apr. 2019, pp. 1–5.
[28] R. MdRafi and A. C. Gurbuz, "Data driven measurement matrix learning for sparse reconstruction," in *Proc. IEEE Data Sci. Workshop*, Jun. 2019, pp. 253–257.
[29] A. Krizhevsky, I. Sutskever, and G. E. Hinton, "Imagenet classification with deep convolutional neural networks," in *Advances in Neural Information Processing Systems 25*, F. Pereira, C. J. C. Burges, L. Bottou, and K. Q. Weinberger, Eds., Red Hook, NY, USA: Curran Associates, Inc., 2012, pp. 1097–1105.
[30] J. Zhang and B. Ghanem, "Ista-net: Iterative shrinkage-thresholding algorithm inspired deep network for image compressive sensing," in *Proc. IEEE Conf. Comput. Vision and Pattern Recognit. (CVPR)*, 2018, pp. 1828–1837.
[31] H. K. Aggarwal, M. P. Mani, and M. Jacob, "MoDL: Model based deep learning architecture for inverse problems," *IEEE Trans. Med. Imag.*, vol. 38, no. 2, pp. 394–405, Feb. 2019.
[32] G. Huang, Z. Liu, L. Van Der Maaten, and K. Q. Weinberger, "Densely connected convolutional networks," in *Proc. Conf. Comput. Vision Pattern Recognit.*, 2017, pp. 2261–2269.
[33] R. C. Gonzalez and R. E. Woods, *Digital Image Processing*. Englewood Cliffs, NJ, USA: Prentice-Hall, 2008.
[34] M. Abadi *et al.*, "TensorFlow: Large-scale machine learning on heterogeneous systems," 2015. Software available from tensorflow.org
[35] T. Blumensath and M. E. Davies, "Iterative hard thresholding for compressed sensing," *Appl. Comput. Harmonic Anal.*, vol. 27, no. 3, pp. 265–274, 2009.
[36] D. Needell and J. A. Tropp, "CoSaMP: Iterative signal recovery from incomplete and inaccurate samples," *Appl. Comp. Harmonic Anal.*, vol. 26, no. 3, pp. 301–321, 2009.
[37] D. L. Donoho, A. Maleki, and A. Montanari, "Message passing algorithms for compressed sensing: I. motivation and construction," in *Proc. IEEE Inf. Theory Workshop Inf. Theory*, Jan. 2010, pp. 1–5.

Robiulhossain Mdrafi (Student Member, IEEE) received the B.Sc. degree in electrical, electronic, and communication engineering from the Bangladesh University of Professionals, Dhaka, Bangladesh, in 2010. He is currently working toward the Ph.D. degree in electrical and computer engineering with Mississippi State University, Starkville, MS, USA. He is a Research Assistant working with the Information Processing and Sensing (IMPRESS) Lab, MS-State. His research interests include deep learning based inverse problems such as sparse signal/image reconstruction, physics aware deep learning and learning in radar and remote sensing applications.

Ali Cafer Gurbuz (Senior Member, IEEE) received the B.S. degree in electrical engineering from Bilkent University, Ankara, Turkey, in 2003, and the M.S. and Ph.D. degrees from the Georgia Institute of Technology, Atlanta, GA, USA, in 2005 and 2008, both in electrical and computer engineering. From 2003 to 2009, he researched compressive sensing based computational imaging problems with Georgia Tech. He held faculty positions with TOBB University and the University of Alabama between 2009 and 2017. He is currently an Assistant Professor with the Department of Electrical and Computer Engineering, Mississippi State University, Starkville, MS, USA, where he is the Co-Director of Information Processing and Sensing (IMPRESS) Lab. His active research program on the development of sparse signal representations, compressive sensing theory and applications, radar and sensor array signal processing, and machine learning. He is the recipient of The Best Paper Award for *Signal Processing Journal* in 2013 and the Turkish Academy of Sciences Best Young Scholar Award in Electrical Engineering in 2014. He was an Associate Editor for several journals such as *Digital Signal Processing*, *EURASIP Journal on Advances in Signal Processing,* and *Physical Communications*. He is a member of Sigma Xi.